Excitation Energy Transfer in Bias-Free Dendrimers: Eigenstate Structure, Thermodynamics and Quantum Evolution

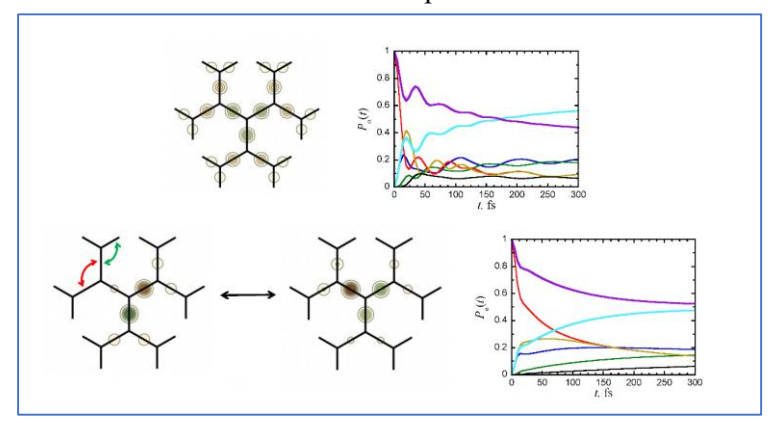
Reshmi Dani¹ and Nancy Makri^{*1,2,3}

¹Department of Chemistry, University of Illinois, Urbana, Illinois 61801

Abstract

We use matrix diagonalization in combination with real-time path integral methods to investigate the electronic eigenstates and exciton-vibration dynamics of model dendrimers with Frenkel exciton interactions between adjacent segments, which characterize structures composed of conjugated molecules. Even in the absence of an explicit energetic gradient in the electronic Hamiltonian, exciton couplings create a funnel through the eigenstate hierarchy which pulls the excitation energy away from the periphery. The competition between eigenstate structure and entropic considerations dictates the equilibrium distribution, which in small dendrimers at low temperatures tends to favor the core, shifting outward with increasing dendrimer size and thermal energy, although this distribution can be skewed back toward the core by increasing the exciton coupling between segments of the same generation. At high temperatures the distribution becomes classical with all excited segments having the same population. Strong exciton-vibration coupling also shifts the equilibrium distribution in the classical direction. We find that the dynamics of excitation energy transfer is highly nontrivial and strongly affected by quantum mechanical effects. A positive value of the intra-generation coupling (regardless of the sign of the inter-generation coupling parameter) introduces a very slow component to the dynamics, which we attribute to electronic frustration. With exciton coupling, vibrational reorganization energy and thermal energy of approximately the same magnitude, the energy transfer dynamics is characterized by time scales that span two orders of magnitude. The rich dynamics that results from a single-parameter electronic Hamiltonian suggests a multitude of design possibilities for dendrimeric structures with desirable function.

TOC Graphic



²Department of Physics, University of Illinois, Urbana, Illinois 61801

³Illinois Quantum Information Science and Technology Center, University of Illinois, Urbana, Illinois 61801

^{*} Email: nmakri@illinois.edu

1. Introduction

The quest for renewable energy has spurred persistent experimental and theoretical activity aiming at designing molecular structures capable of efficient solar energy harvest and storage. Much of this effort has focused on the study of the light harvesting apparatus found in photosynthetic plants and bacteria, which are known to transfer the absorbed light with high efficiency. Ever since their discovery and characterization, ³⁻⁷ light harvesting complexes have been used as prototypes for understanding the complex interplay of electronic states and vibrational motion responsible for this efficiency. Understanding the intricate mechanism of excitation energy transfer (EET) in natural photosynthetic complexes can lead to useful design principles for artificial light harvesting architectures with diverse shapes and topologies. Among many promising candidates, dendrimers have attracted much attention.

Dendrimers are highly branched macromolecules consisting of peripheral groups, repeat units and a core.⁸⁻¹¹ The large volume in relation to their molecular weight allows encapsulation of guest molecules with specific function in their voids, making dendrimers ideal candidates for drug delivery. A judicious choice of building blocks and peripheral functional groups allows control of various important properties, such as density, shape, polarity, chirality, solubility and spectral characteristics. Besides their numerous medical applications, dendrimers are of interest to technology because they can serve as artificial nanoscale antennae. In particular, the funnel-like architecture of dendrimers allows efficient, directional energy transport from the periphery to the core.

Theoretical investigations and simulation can complement experimental work on natural and artificial light harvesting systems and offer invaluable guidance by establishing useful structure-function relations. A variety of theoretical treatments have been employed in the study of excitation energy transfer in natural and synthetic molecular aggregates. ¹²⁻¹⁵ A relatively small body of work has been performed on dendrimers. Theoretical studies have focused primarily on models where each chromophore occupies a lattice site and couples to its nearest neighbors. ¹⁶⁻¹⁹ When the building blocks are conjugated molecules whose wavefunctions are delocalized over linear segments, a better model results by assuming nearest-neighbor interactions between segments. ²⁰ Electronic structure calculations have shown ²⁰ that the interactions between segments can be mapped on the Frenkel exciton Hamiltonian and obtained parameters for the couplings between poly-phenylacetylene units ²¹⁻²² that comprise the nanostar. ⁸ Some explorations of dynamical properties of dendrimer structures have been reported using classical kinetic models, ²³⁻²⁴ quantum mechanical evolution within the electronic subspace studied with exact diagonalization ¹⁷⁻¹⁸ or density matrix renormalization group²⁵ or tree tensor networks ²⁶ and surface hopping approximations. ²⁷⁻³⁰

The kinetics and pathways of EET are governed by the relations among electronic states, molecular vibrations and temperature. The complex interplay of the many energy and time scales found in large molecular structures gives rise to a wide variety of behaviors, which cannot be predicted without accurate, fully quantum mechanical calculations. Several recent developments in quantum dynamics methodology have opened up the road to rigorous and accurate investigations of EET in large molecular systems, where individual intramolecular vibrations play a key role that cannot be captured by simplified treatments. The multilayer multiconfiguration time-dependent Hartree method³¹⁻³² and the time-dependent density matrix renormalization group approach³³ have enabled fully quantum mechanical studies of molecular aggregates comprising several chromophores with a few vibrational modes in each monomer at zero (and in some cases also at a low) temperature. However, the vast size of thermally accessible electronic-vibrational Hilbert space prohibits the use of conventional wavefunction-based approaches when many low-frequency modes are present. Feynman's path integral formulation of offers unique capabilities for treating

large numbers of vibrational degrees of freedom at any temperature. Real-time path integral methods developed in our group⁴⁰⁻⁴⁵ were recently used to investigate EET through all-mode exciton-vibration calculations in the LH2 complex of purple bacteria,⁴⁶⁻⁴⁷ in J aggregates of perylene bisimide⁴⁸⁻⁵⁰ (PBI), in cofacial porphyrin dimers,⁵¹ as well as the coupled spin dynamics of Ising chains interacting with model harmonic baths.⁵² Even though generic characteristics such as decoherence, equilibration, and some aspects of spectral characteristics^{12,53} and density evolution⁵⁴ are common to all these systems and captured through simplified system-bath models,⁵⁵⁻⁵⁶ the striking finding of such all-state, all-mode path integral studies (where the exciton-vibration parameters were treated with their specific molecular values without simplification) is the complexity of the ensuing dynamics and the diversity of observed behaviors.¹⁵

In this paper we use quantum mechanical methods to investigate the eigenstate structure, equilibrium populations, and the EET dynamics in model dendrimers composed of segments interacting via nearest-neighbor Frenkel exciton terms. The Frenkel model⁵⁷ has been found to offer an excellent description of dendrimers composed of conjugated segments.²⁰ Most dendrimer design has focused on utilizing several building blocks with electronic energies that decrease in the direction of the core, in order to create an energy funnel. The latter is understood to be necessary in order to overcome the entropic factor that favors the accumulation of energy in the periphery. Here we explore the possibility of creating structures that enable significant energy flow toward the core in the absence of an energetic bias, and investigate their dynamical behaviors using path integral methods. While the entropic factor may appear to rule out such scenarios, the underlying argument is based on classical thermodynamics and thus ignores the quantum mechanical nature of the dendrimer exciton states. We point out that even in the absence of an energy gradient in the electronic states of the structural units, the population distribution can be manipulated by adjusting the electronic coupling parameters. Such adjustments may be possible through the judicious incorporation of ligands at appropriate locations. One of the benefits of a bias-free funnel architecture is the possibility of quantum coherence and interference, which can allow faster dynamics and possibly alter the EET pathways.

In addition to varying the relative magnitude of intra- vs. inter-generation couplings, we also consider different signs of these parameters. We find that with particular combinations of coupling parameters, the threefold topology of the typical dendrimer gives rise to unusual eigenstate structures dictated by frustration effects similar to those encountered in spin systems. The unusual eigenstate characteristics of such structures are accompanied by significant changes in the dynamics of EET, which becomes considerably slower.

In section 2 we describe the Frenkel exciton Hamiltonian for the dendrimer, including vibrational baths coupled to the ground and excited states of each segment. In section 3 we analyze the electronic eigenstates of the simplest case, a trimer which may represent a dendrimer core (with three identical coupling parameters) or a building block where one segment belongs in one generation while the other two segments belong to another generation. The simple results of this analysis are instructive and help explain the eigenstate structure of larger dendrimers. In section 4 we present numerical results for the electronic eigenstates of a three-generation dendrimer. We also discuss the dependence of the populations of each generation on temperature and dendrimer parameters. The time evolution of the excitation energy is presented in section 5 for representative parameters. Some concluding remarks are given in section 6.

2. Dendrimer Hamiltonian and methods

We focus on dendrimers with coordination number equal to 3, which gives rise to a three-branch structure. We assume that the dendrimer has G generations, each $3 \times 2^{G-1}$ segments, such that the total number of segments is $n = 3(2^G - 1)$ Figure 1 shows a dendrimer comprising two generations (G = 2, n = 9) and a larger one with three generations (G = 3, n = 21). In the larger dendrimer the three innermost segments comprise the core, six segments belong in the second generation, while the twelve outermost segments form the periphery.

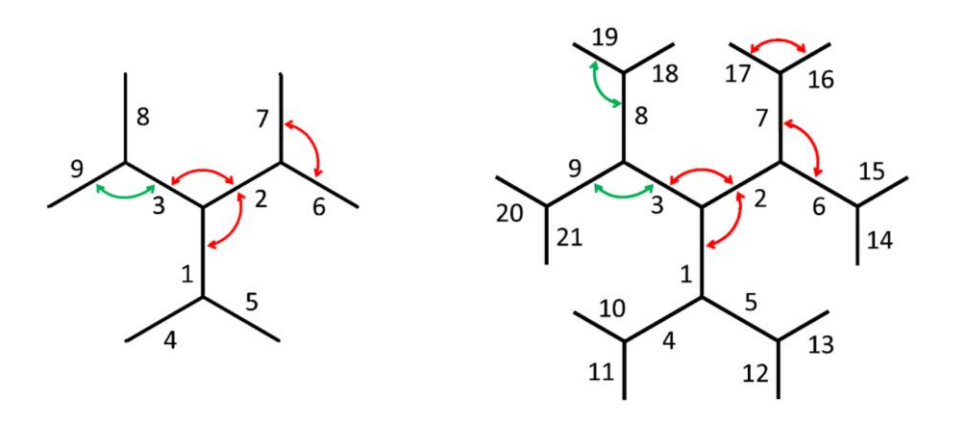


Fig. 1. Two- and three-generation dendrimers (G = 2, n = 9 and G = 3, n = 21). Our numbering of the segments is shown. Intra-generation couplings are shown in red, while inter-generation couplings are shown in green.

Optical excitations in dendrimers made out of conjugated molecules are localized and involve no charge transfer between segments,²¹ so the electronic Hamiltonian has the Frenkel exciton form,⁵⁷

$$\hat{H}_{e} = \sum_{\alpha=1}^{n} \varepsilon_{\alpha} |\alpha\rangle\langle\alpha| + \sum_{\alpha=1}^{n} \sum_{\beta>\alpha}^{n} J_{\alpha\beta} (|\alpha\rangle\langle\beta| + |\beta\rangle\langle\alpha|)$$
(2.1)

where $|\alpha\rangle$ is the state with segment α excited, while all other segments are in the ground state, and $J_{\alpha\beta}$ are the exciton coupling parameters. Following earlier work, we assume that only connected (nearest neighbor) segments are coupled in Eq. (2.1). While the energies of the segments in each generation can vary in general, providing an energy funnel toward the core, in this paper we explore the EET possibilities offered in the absence of an energy bias and set $\varepsilon_{\alpha}=0$. The segment-segment interactions are characterized by two parameters: the coupling J_{intra} between segments within the same generation and the coupling value J_{inter} of nearest-neighbor segments that belong to adjacent generations. Earlier work²² has found that intraand inter-generation couplings can change significantly with small variations of segment length and composition, and that these parameters may have opposite signs within the same dendrimer. We note that

with $J_{\text{intra}} = 0$ the Hamiltonian in Eq. (2.1) describes three unconnected dendra, with eigenvalues that are (at least) three-fold degenerate.

The dynamics of EET is strongly influenced by the coupling of the dendrimer electronic states to intramolecular vibrations. Within the normal mode approximation, the ground and excited electronic states of each segment couple to intramolecular vibrations through the standard Hamiltonian⁵⁸

$$\hat{h}_{\alpha}^{g} = \sum_{i} \left(\frac{\hat{p}_{i\alpha}^{2}}{2m} + \frac{1}{2} m \omega_{i\alpha}^{2} \hat{q}_{i\alpha}^{2} \right), \qquad \hat{h}_{\alpha}^{e} = \sum_{i} \left[\frac{\hat{p}_{i\alpha}^{2}}{2m} + \frac{1}{2} m \omega_{i\alpha}^{2} \left(\hat{q}_{i\alpha} - \frac{c_{i\alpha} s_{e}}{m \omega_{i\alpha}^{2}} \right)^{2} \right]$$

$$(2.2)$$

where $s_{\rm e}$ is a parameter with units of length, $\hat{q}_{i\alpha}$ and $\hat{p}_{i\alpha}$ are the positions and momenta of the normal modes of segment α , and $\omega_{i\alpha}$, $c_{i\alpha}$ are the respective vibrational frequencies and exciton-vibration coupling strengths. The total Hamiltonian is given by

$$\hat{H} = \hat{H}_{e} + \sum_{\alpha=1}^{n} \left(\hat{h}_{\alpha}^{e} + \sum_{\beta \neq \alpha}^{n} \hat{h}_{\beta}^{g} \right) |\alpha\rangle\langle\alpha|.$$
 (2.3)

The effects of molecular vibrations on exciton dynamics are collectively captured through the spectral density function $\mathscr{I}(\omega)$. While the path integral methodology can fully account for vibrational modes characterized by their individual frequencies and coupling coefficients, ¹⁵ in the present model study we employ an Ohmic bath with $\mathscr{I}(\omega) = 2\pi\xi\hbar\omega e^{-\omega/\omega_c}/s_e^2$, where ω_c gives the location of the peak and the dimensionless parameter ξ specifies the exciton-vibration coupling strength. For each segment, the vibrational reorganization energy is given by $\lambda = 2\xi\hbar\omega_c$.

For a chosen electronic excitation, we calculate the time evolution of the $n^2 \times n^2$ electronic reduced density matrix using the small matrix decomposition 43-45 (SMatPI) of the quasi-adiabatic propagator path integral 59-60 (QuAPI). The SMatPI algorithm is an exact decomposition of the fully quantum mechanical real-time path integral expression (which fully accounts for exciton-vibration interactions at any temperature) that employs minimal sized, $n^2 \times n^2$ matrices, thus enabling the simulation of multistate systems. It employs two parameters, the QuAPI memory length L and the entanglement r_{max} . Recent work has shown 61 that the entanglement of the path integral variables may be considerably shorter than the memory length, facilitating convergence in very challenging situations. Representative convergence tests are shown for some of the most challenging cases presented in section 5.

3. The building block

We begin by examining a basic block of a dendrimer, made of three molecular segments as shown in Fig. 2, which interact through the Frenkel exciton Hamiltonian,

$$\hat{H}_{e} = J_{12} (|1\rangle\langle 2| + |2\rangle\langle 1|) + J_{13} (|1\rangle\langle 3| + |3\rangle\langle 1|) + J_{23} (|2\rangle\langle 3| + |3\rangle\langle 2|). \tag{2.4}$$

Because of the symmetry of dendrimer structures, we assume that two of the three exciton coupling parameters are identical and consider the effect of varying the third.

The eigenstates of Eq. (2.4) are easy to obtain and simplify with special choices of the parameters. In the case of an inter-generation block we expect that $J_{12}=J_{13}$, while the third coupling parameter J_{23} may have a different value. The three-segment block that forms the core is characterized by three identical coupling values. We thus set $J_{12}=J_{13}\equiv J$ and examine several characteristic cases, which are illustrated in Fig. 2.

(i) $J_{12} = J_{13} = J$, $J_{23} = 0$. The eigenvalues and corresponding eigenstates are

$$E_{1} = -\sqrt{2} |J|, \quad |\Phi_{1}\rangle = -\frac{\sqrt{2}}{2} \operatorname{sgn}(J) |1\rangle + \frac{1}{2} |2\rangle + \frac{1}{2} |3\rangle$$

$$E_{2} = 0, \quad |\Phi_{2}\rangle = \frac{1}{\sqrt{2}} |2\rangle - \frac{1}{\sqrt{2}} |3\rangle$$

$$E_{3} = +\sqrt{2} |J|, \quad |\Phi_{3}\rangle = +\frac{\sqrt{2}}{2} \operatorname{sgn}(J) |1\rangle + \frac{1}{2} |2\rangle + \frac{1}{2} |3\rangle$$

$$(2.5)$$

The eigenstate density does not depend on the sign of J, but the wavefunctions do. Eq. (2.5) shows that the lowest and highest eigenstates swap upon changing this sign. If J > 0 the ground state wavefunction has opposite amplitudes on the two generations (Fig. 2a), while for J < 0 it is positive throughout the three-segment structure.

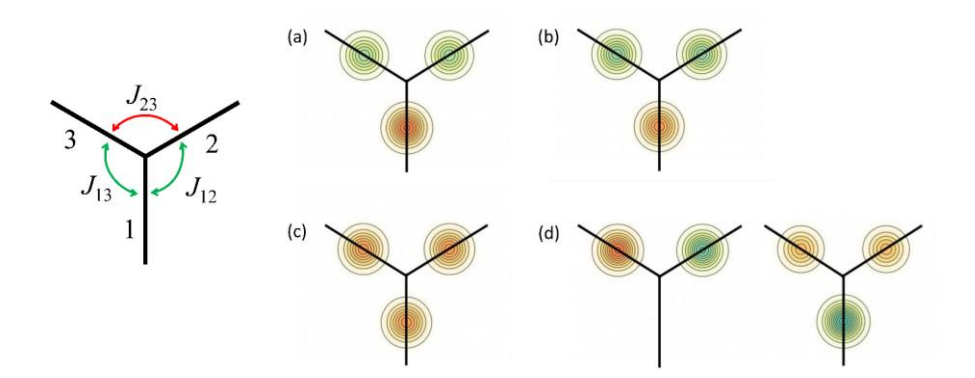


Fig. 2. Left: schematic illustration of three-segment block. Right: visualization of segment amplitudes in the ground state for four combinations of coupling values. The component of the wavefunction on each segment is illustrated by placing a Gaussian of proportional height on the center of the segment. Green and orange indicate positive and negative areas. (a) $J_{12} = J_{13} > 0$, $J_{23} = 0$. (b) $J_{12} = J_{13} > 0$, $J_{23} = -J_{12}$. (c) $J_{12} = J_{13} = J_{23} < 0$. (d) $J_{12} = J_{13} = J_{23} > 0$.

(ii) $J_{12} = J_{13} = J$, $J_{23} = -|J|$. The eigenvalues and eigenstates of Eq. (2.4) are

$$E_{1} = -2|J|, \quad |\Phi_{1}\rangle = -\frac{1}{\sqrt{3}}\operatorname{sgn}(J)|1\rangle + \frac{1}{\sqrt{3}}|2\rangle + \frac{1}{\sqrt{3}}|3\rangle$$

$$E_{2} = |J|, \quad |\Phi_{2}\rangle = \frac{1}{\sqrt{2}}|2\rangle - \frac{1}{\sqrt{2}}|3\rangle$$

$$E_{3} = |J|, \quad |\Phi_{3}\rangle = \frac{2}{\sqrt{6}}\operatorname{sgn}(J)|1\rangle + \frac{1}{\sqrt{6}}|2\rangle + \frac{1}{\sqrt{6}}|3\rangle$$

$$(2.6)$$

With J < 0 (Fig. 2c) all three coupling parameters are identical, thus this condition describes the core of a dendrimer with negative intra-generation coupling, which has a nodeless ground state. The J > 0 case applies to the smallest building block with one segment in one generation and two in the next generation (Fig. 2b). This trimer has a ground state wavefunction that switches sign across generations, and a pair of degenerate excited states. The negative intra-generation coupling stabilizes the system.

(iii) $J_{12} = J_{13} = J_{23} = J > 0$. In this case (Fig. 2d) we find

$$E_{1} = -J, \quad |\Phi_{1}\rangle = -\frac{2}{\sqrt{6}}|1\rangle + \frac{1}{\sqrt{6}}|2\rangle + \frac{1}{\sqrt{6}}|3\rangle$$

$$E_{2} = -J, \quad |\Phi_{2}\rangle = \frac{1}{\sqrt{2}}|2\rangle - \frac{1}{\sqrt{2}}|3\rangle$$

$$E_{3} = 2J, \quad |\Phi_{3}\rangle = \frac{1}{\sqrt{6}}|1\rangle + \frac{1}{\sqrt{6}}|2\rangle + \frac{1}{\sqrt{6}}|3\rangle$$

$$(2.7)$$

The ground state is now doubly degenerate, and is destabilized. This structure exhibits frustration, an effect familiar from interacting spin systems: the positive inter-generation couplings favor opposite signs, forcing the outer generation segments 2 and 3 to have the same sign, an unfavorable arrangement for $J_{23} > 0$.

When all three couplings have the same magnitude equal to J, the evolution of electronic populations following excitation of one segment is given by

$$P_{\alpha}(t) = \frac{1}{9} \left[5 + 4\cos(3Jt/\hbar) \right],$$
 (2.8)

regardless of the relative signs.

To summarize this section, eigenstate densities are insensitive to the sign of the two identical (intergeneration) couplings in a trimer, but the spectrum and the ground state structure change drastically when the third coupling (between segments within the same generation) reverses sign. A negative intra-generation stabilizes the structure, while a positive value destabilizes the system and gives rise to a pair of degenerate ground states. We now turn to larger dendrimers and use numerical diagonalization to study the eigenstates of the electronic Hamiltonian.

4. Eigenvectors and equilibrium distributions

In this section we investigate the eigenstate structure and equilibrium populations of dendrimer of varying size. We set $J_{\rm inter} = J > 0$, but consider different magnitudes and signs of $J_{\rm intra}$. In each case we examine the wavefunction of the ground state(s) and of select excited states for three-generation dendrimers. In addition, we show the total populations of excited segments that comprise each generation of the electronic Hamiltonian, at zero temperature and also at $k_{\rm B}T = 0.2J$, J, and 10J, for two-, three-, and four-generation dendrimers. The first of the finite temperatures is very low for typical values of the inter-generation coupling (50-500 cm⁻¹). Yet, we find that with particular choices of $J_{\rm intra}$, the populations are drastically different from those obtained at zero temperature. With $k_{\rm B}T = 10J$ the electronic Hamiltonian of the dendrimer is in the high-temperature regime for all exciton coupling values considered here. In this case all segments have equal populations, and thus each generation has twice as many segments as the previous one. Statistical and dynamical results obtained within classical hopping assumptions²³⁻²⁴

pertain to this high-temperature limit. As is seen in the figures presented in this section, the quantized electronic Hamiltonian of the dendrimer gives rise to entirely different population distributions at low and intermediate temperatures. It is natural to expect that quantum effects will be very prominent in the dynamics of exciton-vibration dynamics and the EET evolution as well.

(i) All $J_{\text{intra}} = 0$. Since the core segments are not connected, this structure consists of three separate dendra. The eigenstates of the Hamiltonian exhibit a threefold degeneracy in this case. With proper linear combinations, the wavefunctions are delocalized over the entire dendrimer. Figure 3 shows that the ground state wavefunctions have circular nodes between generations, while the highest lying states are nodeless.

The total population generations at zero temperature (also shown in Fig. 3) are distributed symmetrically, with the largest populations found in the middle generation(s). The highest core population is found in the G=2 dendrimer, where it is equal to only ½. The distribution becomes skewed when temperature is introduced, and its maximum shifts toward the periphery. Even at the intermediate temperature $k_BT=J$, the generation populations of large dendrimers (G>4) approach a classical-like distribution.

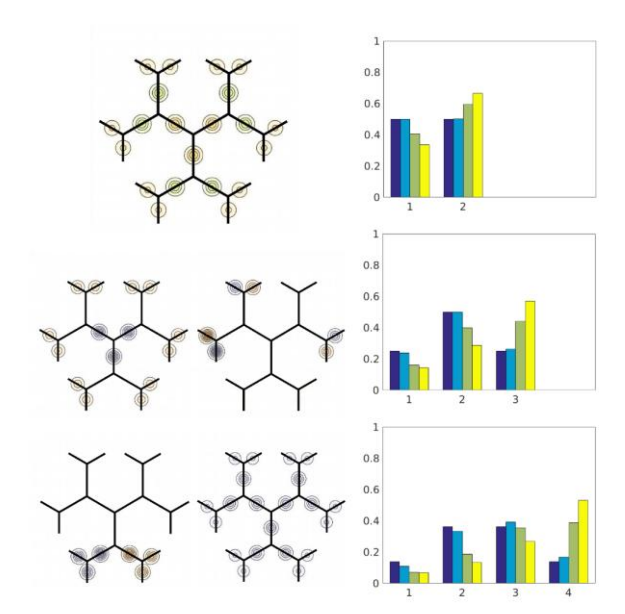


Fig. 3. Visualization of segment amplitudes and population distribution for $J_{\text{intra}}=0$. Left: eigenstate amplitudes on the various segments for a three-generation dendrimer. All eigenstates are threefold degenerate here. The larger image shows the ground state Φ_1 , while the four smaller images show eigenstates Φ_7 , Φ_{12} , Φ_{16} , and Φ_{19} (which has the largest eigenvalue). Orange/green and blue/orange correspond to positive and negative amplitudes. Right: total population of each generation for dendrimers with two, three and four generations at various temperatures. Dark blue: T=0. Cyan: $k_BT=0.2J$. Green: $k_BT=J$. Yellow: $k_BT=10J$.

(ii) $J_{\rm intra} < 0$. In this case the eigenstates maintain the spreading and alternating sign features observed with $J_{\rm intra} = 0$, but the threefold degeneracy is lifted. Figure 4 shows the eigenfunctions and equilibrium population distributions for $J_{\rm intra} = -J$ and -3J. As expected based on the analysis presented in the previous section, increasing intra-generation coupling stabilizes the dendrimer, lowering the ground state energy and increasing the population of core segments. With these values of $J_{\rm intra}$, small dendrimers have

their largest populations in the core at zero temperature. As expected, the generation populations depend nonmonotonically on generation number as the temperature is increased, eventually approaching the statistical limit. In large dendrimers, the entropic effect becomes noticeable at low temperatures, although this effect is countered by increasing the value of $J_{\rm intra}$, which shifts more population toward innermost segments. With $J_{\rm intra} = -3J$ the core population is maintained above or slightly below 0.8 for the G = 2,3,4 dendrimers examined. With negative intra-generation coupling, temperature has a gradual effect on excitation distribution among generations, with the core population at $k_{\rm B}T = 0.2J$ remaining almost equal to that at zero temperature even in all three dendrimers.

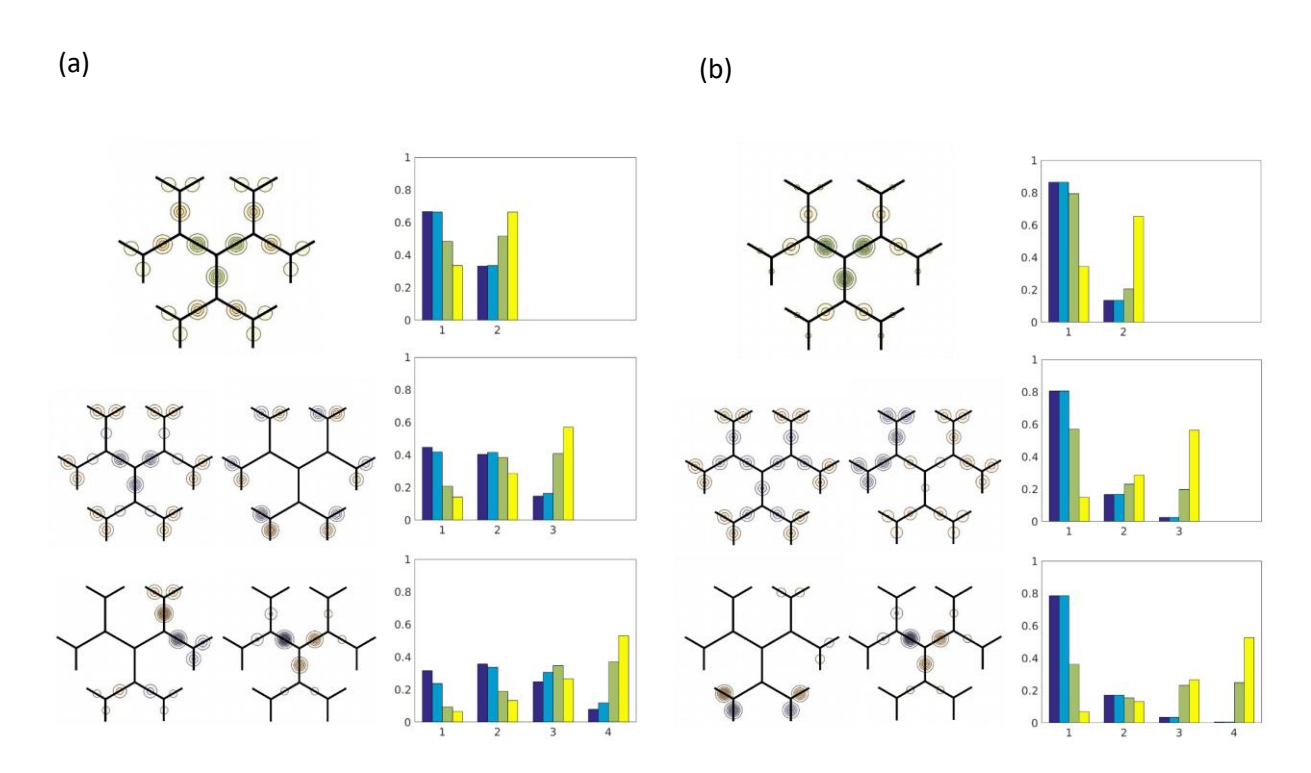


Fig. 4. Visualization of segment amplitudes and population distribution for (a) $J_{\text{intra}} = -J$ and (b) $J_{\text{intra}} = -3J$. Left: eigenstate amplitudes on the various segments for a three-generation dendrimer. The larger image shows the ground state Φ_1 , while the four smaller images show eigenstates (a) Φ_7 , Φ_{11} , Φ_{18} , Φ_{20} and (b) Φ_4 , Φ_9 , Φ_{16} , Φ_{20} . Orange/green and blue/orange correspond to positive and negative amplitudes. Right: total population of each generation for dendrimers with two, three and four generations at various temperatures. Dark blue: T = 0. Cyan: $k_B T = 0.2J$. Green: $k_B T = J$. Yellow: $k_B T = 10J$.

(iii) $J_{\text{intra}} > 0$. The picture changes dramatically when the intra-generation couplings are positive. Figure 5 shows results with all $J_{\text{intra}} = J$ or 3J. In analogy with the three-segment Hamiltonians examined in the previous section, the three-branch dendrimer has two degenerate ground states that do not reflect the threefold symmetry of the dendrimer structure. Again, this is the result of frustration within each generation. As seen in Fig. 5, one of the two degenerate ground states is now distributed on only two of the three dendrimer branches. The excitation distribution across the three generations is the complex outcome of a competition between frustration and delocalization. This competition pushes the ground state density toward the core, attempting to minimize population on the periphery which has the largest number of

unfavorably interacting segments. As a result, the entropic effect aids core accumulation of the excitation energy at zero temperature. Fig. 5 shows that the T=0 core population is larger here in comparison to equivalent cases with $J_{\rm intra} < 0$, and it increases with increasing $J_{\rm intra}$. Further, the shift of excitation population away from the core with increasing dendrimer size is considerably weaker in the present case, showing almost no change if $J_{\rm intra} = 3J$.

However, there are now eigenstates with large density in the second generation, which are nearly degenerate with the ground states. These eigenstates are rapidly populated upon increasing the temperature, depleting the population of core segments. Even at the very low temperature $k_{\rm B}T=0.2J$ the core population with $J_{\rm intra}=3J$ drops to about 0.15, compared to 0.95 at T=0, and the maximum population is found in the third generation. Thus, while the equilibrium distribution of excited state populations is overall larger with $J_{\rm intra}>0$ in comparison to identical dendrimers with negative intra-generation couplings, the trend reverses rapidly when finite temperature is introduced, and the excitation energy approaches the statistical limit faster in this case.

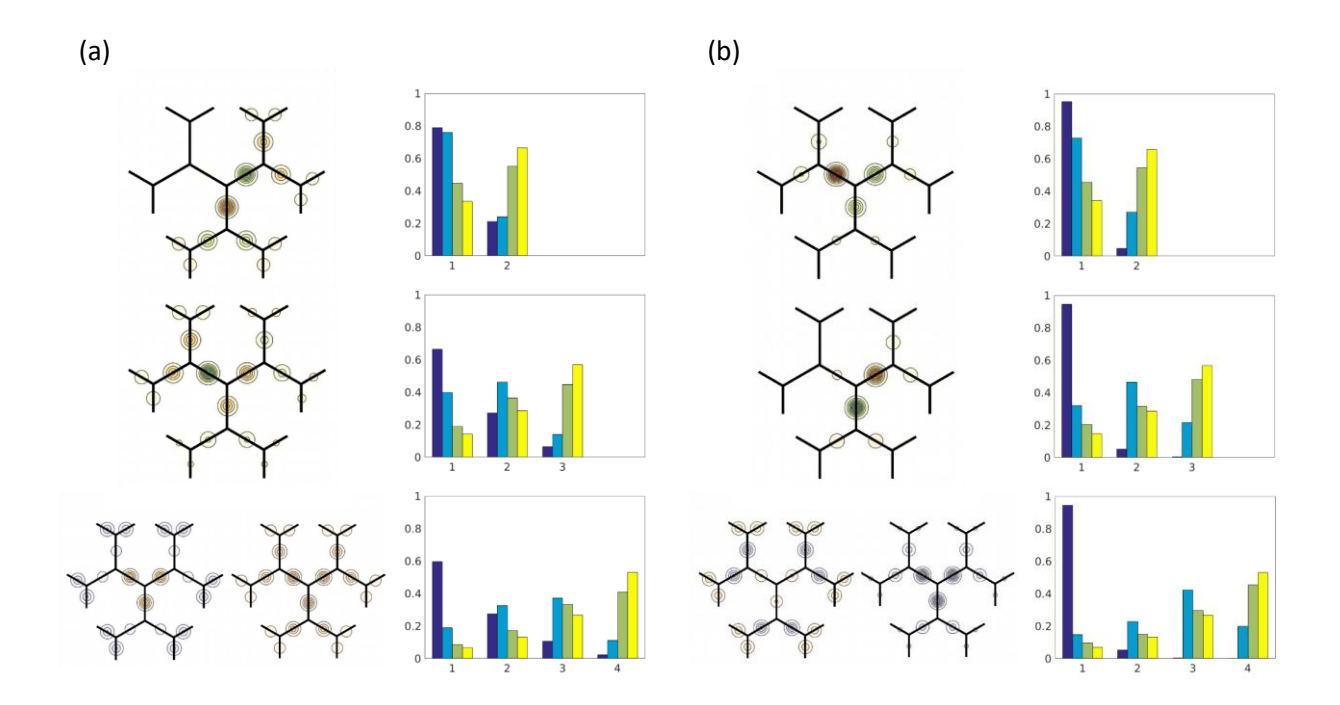


Fig. 5. Visualization of segment amplitudes and population distribution for (a) $J_{\text{intra}} = +J$ and (b) $J_{\text{intra}} = +3J$. Left: eigenstate amplitudes on the various segments for a three-generation dendrimer. The larger images show the two degenerate ground states Φ_1 and Φ_2 , while the two smaller images show excited eigenstates (a) Φ_{15} , Φ_{21} and (b) Φ_{12} , Φ_{21} . Orange/green and blue/orange correspond to positive and negative amplitudes. Right: total population of each generation for dendrimers with two, three and four generations at various temperatures. Dark blue: T=0. Cyan: $k_BT=0.2J$. Green: $k_BT=J$. Yellow: $k_BT=10J$.

5. Dynamics of excitation energy transfer

We now turn to the time evolution of the excitation energy following excitation of a segment located in the periphery. The population evolution does not depend on the sign of the inter-generation

coupling. We thus fix the value of this coupling to $J_{\rm inter}=J=300~{\rm cm}^{-1}$ (a value in the range expected for such systems) and consider a positive and a negative intra-generation coupling, $J_{\rm intra}=\pm300~{\rm cm}^{-1}$. Further, we assume that the vibrational spectral density peaks at $\omega_{\rm c}=1500~{\rm cm}^{-1}$ and examine the dynamics for two values of the reorganization energy, a moderate value $\lambda=J=300~{\rm cm}^{-1}$ and a large value $900~{\rm cm}^{-1}$. After examining the simpler trimer at $100~{\rm K}$ for each parameter combination, we present results for the G=2 dendrimer at $T=100~{\rm K}$ (which corresponds to $J/k_{\rm B}T=4.31$) and $300~{\rm K}$ ($J/k_{\rm B}T=1.44$).

We begin by investigating the dynamics of the two relevant trimer structures examined in section III (Fig. 2b and 2d) where two of the segments are connected through $J_{\rm inter}$ while the third pair couples through $J_{\rm intra}=\pm300~{\rm cm}^{-1}$. Figure 6 shows the populations of the excited segments as a function of time at 100 K. In all cases the excitation relaxes fairly rapidly (within 0.5 ps) to its equilibrium value, which equals 1/3 for all three segments. However, significant differences are observed among the four cases. With the weaker exciton-vibration coupling ($\lambda=300~{\rm cm}^{-1}$), the EET dynamics is coherent (underdamped), more so with $J_{\rm intra}<0$, but the oscillatory behavior is lost upon increasing the reorganization energy to $900~{\rm cm}^{-1}$. Even though we only show results at $100~{\rm K}$ for this system, we note that only a mild reduction in the oscillatory patterns is observed upon increasing the temperature to $300~{\rm K}$. While this temperature is intermediate in relation to the exciton coupling parameters, it is low with respect to the vibrational frequencies, thus providing inadequate damping.

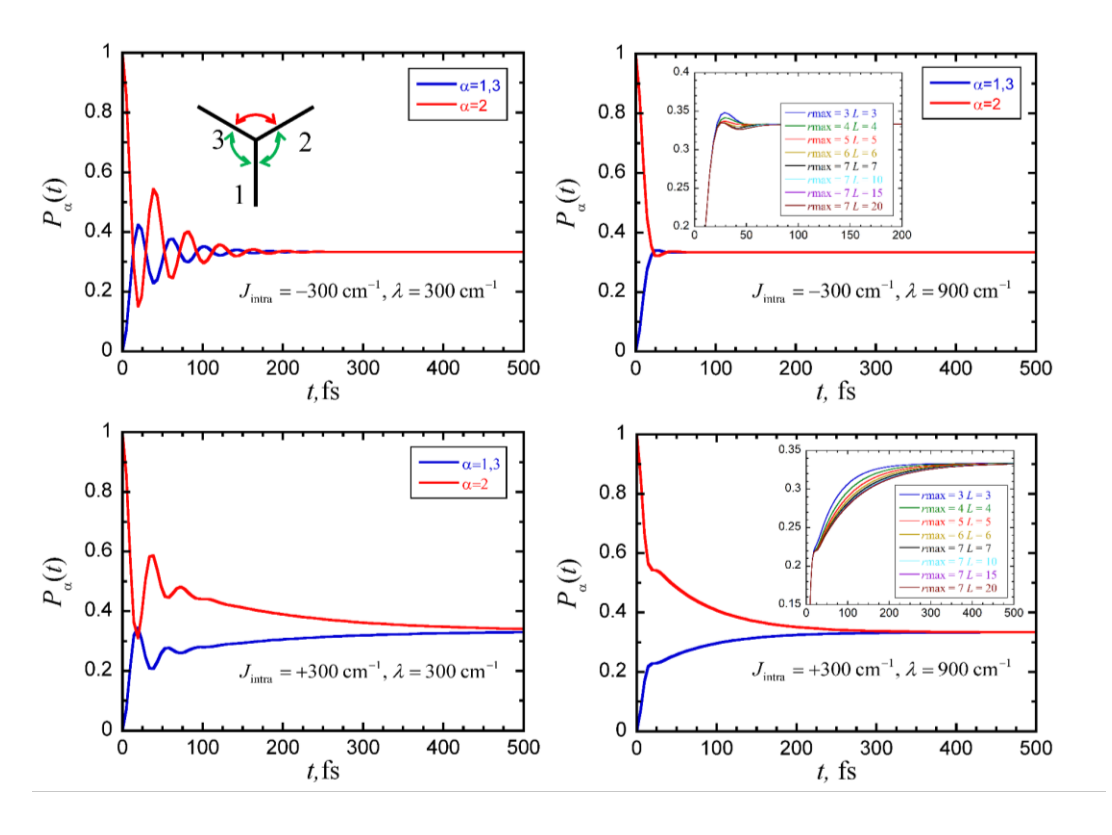


Fig. 6. Excited segment populations as a function of time following excitation of segment 2 for a trimer with the parameters given in the text at 100 K. For convenience we show the dendrimer structure with segment numbers in one of the panels, where red and green arrows indicate the couplings J_{inter} and J_{inter} , respectively. The insets show the convergence of P_{l} for various values of the SMatPI entanglement length T_{max} and memory length T_{length} .

Perhaps the most striking contrast observed in Fig. 6 is the lengthening of the EET relaxation time when $J_{\rm intra}>0$, compared to the dynamics with $J_{\rm intra}<0$ (of the same magnitude) and all other parameters fixed. Two distinct time scales can be identified in the dynamics with $J_{\rm intra}>0$, which are most clearly seen in the results with $\lambda=900~{\rm cm}^{-1}$. Regardless of the sign of $J_{\rm intra}$, a fast population transfer out of the initially excited state is observed during the initial 15 fs. The subsequent evolution is also rapid and unremarkable when $J_{\rm intra}<0$, and the population settles to its equilibrium value within approximately 50 fs. In sharp contrast, when $J_{\rm intra}>0$ the population transitions to a slow decay, reaching equilibrium at approximately 300 fs (a sixfold slowdown). The relaxation is even slower with the smaller reorganization energy $\lambda=300~{\rm cm}^{-1}$, and energy transfer lasts 0.5 ps in this case.

Interestingly, as discussed in section III, the EET dynamics resulting with different signs of $J_{\rm intra}$ are identical in the absence of exciton-vibration coupling. The unexpected behavior observed with $J_{\rm intra} > 0$ is a consequence of frustration that manifests itself only when interaction with vibrational degrees of freedom enables the excitation energy to equilibrate within the dendrimer, a process that involves a redistribution of population between degenerate ground states. Such a process is enabled by the vibrational bath and tends to be very slow.

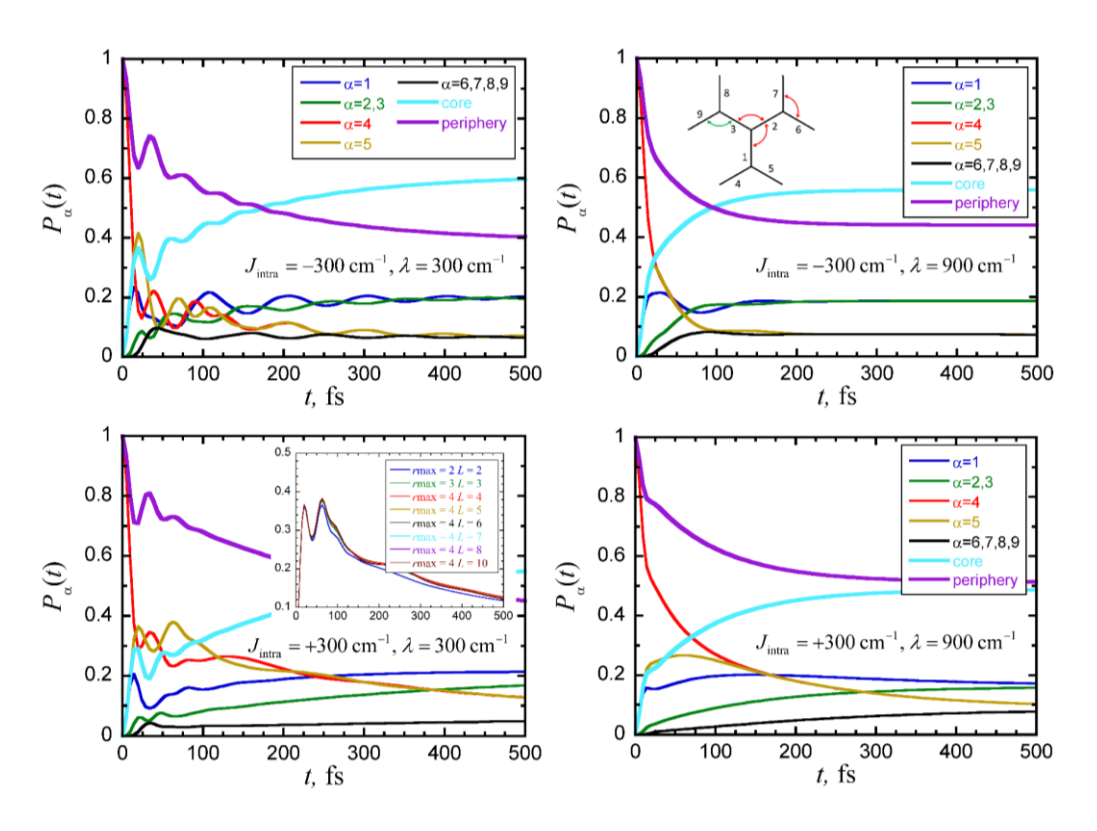


Fig. 7. Energy transfer dynamics in G=2 dendrimers with the parameters given in the text at T=100 K. For convenience we show the dendrimer structure with segment numbers in one of the panels. The inset shows the convergence of $P_{\rm s}$ for various values of the SMatPI entanglement length $r_{\rm max}$ and memory length L.

Several of these trends are observed in the larger G=2 dendrimers whose EET evolution is shown in Figures 7-9 at three temperatures, although the coherence patterns are more complex here since they are governed by multiple energy scales associated with the n=9 electronic eigenvalues, and the EET process lasts longer. Starting with the excitation in the peripheral segment 4, the energy rapidly spreads to the neighboring segments 1 and 5. A preferential population accumulation on the terminal unit 5 is observed at early times, as segment 1 is continuously depleted through subsequent transfer to the other two core units. The populations of distant peripheral segments increase gradually and with a short delay.

The dynamics with $J_{\rm intra} = -300~{\rm cm}^{-1}$ is fast here too, but the amplitude of the oscillations in the population evolution at 100 K is now smaller than in the three-segment dendrimer, in line with similar observations in large molecular aggregates. However, with the smaller reorganization energy $\lambda = 300~{\rm cm}^{-1}$, small-amplitude coherent oscillations survive much longer (up to 500 fs) in this larger dendrimer. With the larger reorganization energy, equilibration is reached in approximately 200 fs. In this larger dendrimer, positive values of the intra-generation coupling lead to even slower energy transfer, although the strikingly different dynamical patterns compared to those with negative coupling are less conspicuous here. With $J_{\rm intra} = 300~{\rm cm}^{-1}$ the populations reach their equilibrium values around 1.5 ps (although, for consistency, we only show the initial 500 fs in the figure).

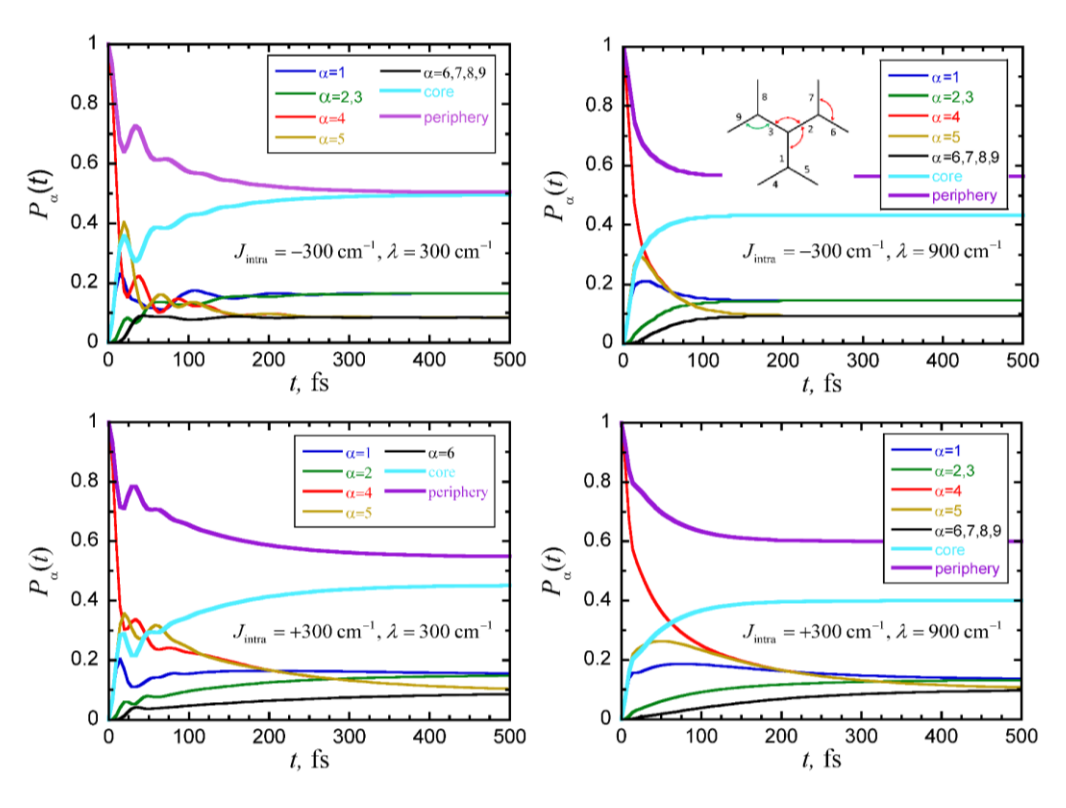


Fig. 8. Energy transfer dynamics in G = 2 dendrimers with the parameters given in the text at T = 300 K. For convenience we show the dendrimer structure with segment numbers in one of the panels.

The EET evolution at higher temperatures is faster and the transfer of energy to the core is progressively diminished. At $T = 1000 \, \text{K}$ (Fig. 9) the long-time population of the core is almost equal to

its classical value. Remarkably, even under these nearly classical conditions, the quantum mechanical nature of the electronic system is clearly noticeable. This eigenstate structure and in particular the effects of frustration associated with positive intra-generation coupling are still seen to give rise to considerably slower dynamics, with the core population taking approximately twice as long to reach its reaching its equilibrium value in comparison to the $J_{\rm intra}$ < 0 case.

The role of nuclear motion on the dynamics of EET in these dendrimers is also intriguing. In addition to their coherence-damping function, intramolecular vibrations are seen to significantly perturb the equilibrium distribution of excited segment populations. This effect is clearly seen at 100 and 300 K, where the long-time distribution of excitation energy between core and periphery is closer to the statistical limit when the reorganization energy has the large value $\lambda = 900 \, \mathrm{cm}^{-1}$ than with the smaller exciton-vibration coupling for which $\lambda = 300 \, \mathrm{cm}^{-1}$. A strong coupling of the electronic states to vibrational motion results in overall more classical-like behavior, which is expressed not only through the damping of electronic coherence but also in terms of the population distribution at thermal equilibrium.

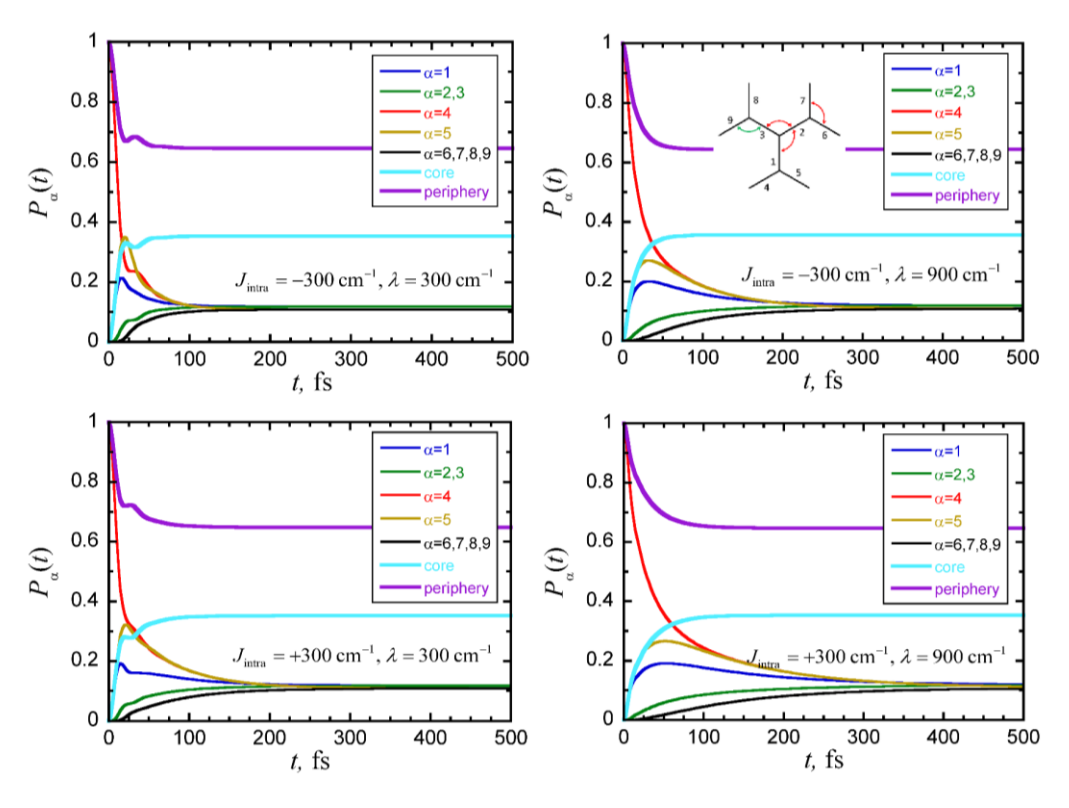


Fig. 9. Energy transfer dynamics in G = 2 dendrimers with the parameters given in the text at T = 1000 K. For convenience we show the dendrimer structure with segment numbers in one of the panels.

6. Concluding Remarks

In this paper we have investigated the quantum mechanical structure, equilibrium properties and real-time dynamics of dendrimers described by a simple Frenkel exciton model with interaction between bias-free nearest-neighbor segments coupled to model vibrational baths. By refraining from creating an energy funnel though a downhill arrangement of chromophore energies, we were able to focus on the rich

interplay among quantum coherence, topology, entropic factors, exciton-vibration interactions and temperature, identifying intriguing behaviors.

Even within the confines of the present single-parameter electronic Hamiltonian, several of these findings point to the remarkable physics of dendrimeric structures and the endless possibilities for targeted function through nanoscale design. Perhaps the first notable result is that even in the absence of an energetic funnel built into the electronic Hamiltonian, these structures are able to transfer excitation energy from the periphery to the core. This function is a consequence of quantum effects, which give rise to eigenstate structures and equilibrium distributions that can favor the core at low temperatures. We find that when the electronic coupling parameters are fixed, small dendrimers have largest populations in the core, and that the peak of the distribution gradually shifts outward with increasing size. However, for a given dendrimer size, the core population can be increased by increasing the intra-generation coupling (or, equivalently, decreasing the inter-generation coupling strength). Thus, electronic coupling can counter the periphery-favoring entropic factor, achieving outcomes that are vastly different from those based on classical statistical models.

The eigenstate structure of these dendrimers is dominated by the sign of the intra-generation coupling parameter. By analyzing a basic trimeric building block, we found that a positive value of this parameter gives rise to a destabilized structure with a doubly degenerate ground state whose wavefunction does not exhibit the threefold symmetry of the dendrimer. We attributed this effect to electronic frustration, in analogy to the analogous effect known from spin systems. The unfavorable interaction generated by an odd number of positive couplings within a three-state unit effectively shifts electronic density toward the core, further countering the entropic effect at zero temperature. At the same time, the close proximity of multiple low-lying states leads to a sharp drop of core population upon increasing the temperature even slightly. The dynamical manifestations of electronic frustration are surprising and remarkable. We found that EET slows down very significantly when the intra-generation coupling is positive, in comparison with situations where this parameter has the same magnitude but a negative sign.

Exciton-vibration interactions play a major role in EET and are required for equilibration and the trapping of energy. With small-to-moderate values of the vibrational reorganization energy ($\lambda \simeq J$) the population evolution is underdamped. More efficient quenching of oscillatory features is observed in dendrimers with positive intra-generation coupling. Increasing exciton-vibration coupling causes a shift of equilibrium populations away from the core, as the composite system becomes effectively more classical.

Thermal effects wash out phase relations and effects related to quantized level structure. Upon increasing the temperature, the population distribution becomes more classical-like, with each segment having a population equal to 1/n in the infinite temperature limit. Interestingly, dynamical features such as those related to the sign of intra-generation couplings persist to sufficiently high temperatures, even though the equilibrium populations are close to their classical values. With typical Frenkel couplings of the order of $200-300\,\mathrm{cm}^{-1}$, the temperatures required for classical-like behavior are extremely high, thus quantum effects are expected to be prominent in dendrimers at or below physiological temperatures.

Overall, using a simple model with a single electronic parameter of fixed magnitude ($|J| = 300 \, \mathrm{cm}^{-1}$) and two possible values of vibrational reorganization energy ($\lambda = |J|$ or $\lambda = 3|J|$), our calculations identified a vast range of time scales in the EET dynamics of G=2 dendrimers at a fixed temperature, ranging from a 15 fs ultrafast transfer out of the initially excited peripheral segment to a slow 1.5 ps equilibration, which span two orders of magnitude. These very rich behaviors will undoubtedly become

even more complex when additional parameters are allowed to vary, inviting additional work on these fascinating systems.

Acknowledgments

This material is based upon work supported by the National Science Foundation under Award CHE-1955302. We thank Sohang Kundu for making his SMatPI code available for this work.

References

- 1. Pullerits, T.; Sundstrom, V., Photosynthetic light-harvesting pigment-protein complexes: Toward understanding how and why. *Acc. Chem. Res.* **1996**, *29*, 381-389.
- 2. Blankenship, R. E., *Molecular mechanisms of photosynthesis*. World Scientific: London, 2002.
- 3. van Grondelle, R.; Dekker, J. P.; Gillbro, T.; Sundstrom, V., Energy transfer and trapping in photosynthesis. *Biochim. Biophys. Acta* **1994**, *1187*, 1-65.
- 4. McDermott, G.; Prince, S.; Freer, A.; Hawthornthwaite-Lawless, A.; Papiz, M.; Cogdell, R.; Isaacs, N., Crystal structure of an integral membrane light-harvesting complex from photosynthetic bacteria. *Nature* **1995**, *374*, 517.
- 5. Hu, X.; Xu, D.; Hamer, K.; Schulten, K.; Koepke, J.; Michel, H., Predicting the structure of the light harvesting complex II of rhodospirillum molischianum. *Protein Science* **1995**, *4*, 1670-1682.
- 6. Koepke, J.; Hu, X.; Muenke, C.; Schulten, K.; Michel, H., The crystal structure of the light harvesting complex II (B800-B850) from Rhodospirillum molischianum. *Structures* **1996**, *4*, 581-597.
- 7. Cogdell, R. J.; Isaacs, N. W.; Freer, A. A.; Arrelano, J.; Howard, T. D.; Papiz, M. Z.; Hawthornthwaite-Lawless, A. M.; Prince, S., The structure and function of the LH2 (B800–850) complex from the purple photosynthetic bacterium Rhodopseudomonas acidophila strain 10050. *Progress in Biophysics and Molecular Biology* **1997**, *68* (1), 1-27.
- 8. Moore, J. S., Shape-Persistent Molecular Architectures of Nanoscale Dimension. *Accounts of Chemical Research* **1997**, *30* (10), 402-413.
- 9. Ballauff, M.; Likos, C. N., Dendrimers in Solution: Insight from Theory and Simulation. *Angewandte Chemie International Edition* **2004**, *43* (23), 2998-3020.
- 10. Astruc, D.; Boisselier, E.; Ornelas, C., Dendrimers Designed for Functions: From Physical, Photophysical, and Supramolecular Properties to Applications in Sensing, Catalysis, Molecular Electronics, Photonics, and Nanomedicine. *Chemical Reviews* **2010**, *110* (4), 1857-1959.
- 11. Abbasi, E.; Aval, S. F.; Akbarzadeh, A.; Milani, M.; Nasrabadi, H. T.; Joo, S. W.; Hanifehpour, Y.; Nejati-Koshki, K.; Pashaei-Asl, R., Dendrimers: synthesis, applications, and properties. *Nanoscale Research Letters* **2014**, *9* (1), 247.
- 12. Schröter, M.; Ivanov, S. D.; Schulze, J.; Polyutov, S. P.; Yan, Y.; Pullerits, T.; Kühn, O., Exciton–vibrational coupling in the dynamics and spectroscopy of Frenkel excitons in molecular aggregates. *Physics Reports* **2015**, *567*, 1-78.
- 13. Hestand, N. J.; Spano, F. C., Expanded Theory of H- and J-Molecular Aggregates: The Effects of Vibronic Coupling and Intermolecular Charge Transfer. *Chemical Reviews* **2018**, *118* (15), 7069-7163.
- 14. Popp, W.; Brey, D.; Binder, R.; Burghardt, I., Quantum Dynamics of Exciton Transport and Dissociation in Multichromophoric Systems. *Annual Review of Physical Chemistry* **2021**, *72* (1), 591-616.
- 15. Kundu, S.; Makri, N., Intramolecular Vibrations in Excitation Energy Transfer: Insights from Real-Time Path Integral Calculations. *Annual Review of Physical Chemistry* **2022**, *73* (1), 349-375.
- 16. Harigaya, K., Coupled exciton model with off-diagonal disorder for optical excitations in extended dendrimers. *Physical Chemistry Chemical Physics* **1999**, *1* (7), 1687-1689.
- 17. Mülken, O.; Blumen, A., Slow transport by continuous time quantum walks. *Physical Review E* **2005,** *71* (1), 016101.
- 18. Mülken, O.; Bierbaum, V.; Blumen, A., Coherent exciton transport in dendrimers and continuous-time quantum walks. *The Journal of Chemical Physics* **2006**, *124* (12), 124905.
- 19. Pouthier, V., Exciton localization-delocalization transition in an extended dendrimer. *The Journal of Chemical Physics* **2013**, *139* (23), 234111.
- 20. Poliakov, E. Y.; Chernyak, V.; Tretiak, S.; Mukamel, S., Exciton-scaling and optical excitations of self-similar phenylacetylene dendrimers. *The Journal of Chemical Physics* **1999**, *110* (16), 8161-8175.
- 21. Tretiak, S.; Chernyak, V.; Mukamel, S., Localized Electronic Excitations in Phenylacetylene Dendrimers. *The Journal of Physical Chemistry B* **1998**, *102* (18), 3310-3315.

- 22. Minami, T.; Tretiak, S.; Chernyak, V.; Mukamel, S., Frenkel-exciton Hamiltonian for dendrimeric nanostar. *Journal of Luminescence* **2000**, *87-89*, 115-118.
- 23. Bar-Haim, A.; Klafter, J.; Kopelman, R., Dendrimers as Controlled Artificial Energy Antennae. *Journal of the American Chemical Society* **1997**, *119* (26), 6197-6198.
- 24. Bar-Haim, A.; Klafter, J., Geometric versus Energetic Competition in Light Harvesting by Dendrimers. *The Journal of Physical Chemistry B* **1998**, *102* (10), 1662-1664.
- 25. Martín-Delgado, M. A.; Rodriguez-Laguna, J.; Sierra, G., Density-matrix renormalization-group study of excitons in dendrimers. *Physical Review B* **2002**, *65* (15), 155116.
- 26. Nagy, Á., Simulating quantum systems on the Bethe lattice by translationally invariant infinite-tree tensor network. *Annals of Physics* **2012**, *327* (2), 542-552.
- 27. Fernandez-Alberti, S.; Kleiman, V. D.; Tretiak, S.; Roitberg, A. E., Nonadiabatic Molecular Dynamics Simulations of the Energy Transfer between Building Blocks in a Phenylene Ethynylene Dendrimer. *The Journal of Physical Chemistry A* **2009**, *113* (26), 7535-7542.
- 28. Soler, M. A.; Roitberg, A. E.; Nelson, T.; Tretiak, S.; Fernandez-Alberti, S., Analysis of State-Specific Vibrations Coupled to the Unidirectional Energy Transfer in Conjugated Dendrimers. *The Journal of Physical Chemistry A* **2012**, *116* (40), 9802-9810.
- 29. Galindo, J. F.; Atas, E.; Altan, A.; Kuroda, D. G.; Fernandez-Alberti, S.; Tretiak, S.; Roitberg, A. E.; Kleiman, V. D., Dynamics of Energy Transfer in a Conjugated Dendrimer Driven by Ultrafast Localization of Excitations. *Journal of the American Chemical Society* **2015**, *137* (36), 11637-11644.
- 30. Ondarse-Alvarez, D.; Oldani, N.; Roitberg, A. E.; Kleiman, V.; Tretiak, S.; Fernandez-Alberti, S., Energy transfer and spatial scrambling of an exciton in a conjugated dendrimer. *Physical Chemistry Chemical Physics* **2018**, *20* (47), 29648-29660.
- 31. Beck, M. H.; Jäckle, A.; Worth, G. A.; Meyer, H.-D., The multiconfiguration time-dependent Hartree (MCTDH) method: a highly efficient algorithm for propagating wavepackets. *Phys. Rep.* **2000**, *324*, 1-105.
- 32. Wang, H.; Thoss, M., Multilayer formulation of the multiconfiguration time-dependent Hartree theory. *The Journal of Chemical Physics* **2003**, *119* (3), 1289-1299.
- 33. Schollwöck, U., The density-matrix renormalization group in the age of matrix product states. *Annals of Physics* **2011**, *326*, 96-192.
- 34. Ambrosek, D.; Marciniak, H.; Lochbrunner, S.; Tatchen, J.; Li, X.-Q.; Würthner, F.; Kühn, O., Photophysical and quantum chemical study on a J-aggregate forming perylene bisimide monomer. *Physical Chemistry Chemical Physics* **2011**, *13* (39), 17649-17657.
- 35. Popp, W.; Polkehn, M.; Hughes, K. H.; Martinazzo, R.; Burghardt, I., Vibronic coupling models for donor-acceptor aggregates using an effective-mode scheme: Application to mixed Frenkel and charge-transfer excitons in oligothiophene aggregates. *The Journal of Chemical Physics* **2019**, *150* (24), 244114.
- 36. Ren, J.; Shuai, Z.; Kin-Lic Chan, G., Time-Dependent Density Matrix Renormalization Group Algorithms for Nearly Exact Absorption and Fluorescence Spectra of Molecular Aggregates at Both Zero and Finite Temperature. *Journal of Chemical Theory and Computation* **2018**, *14* (10), 5027-5039.
- 37. Feynman, R. P., Space-time approach to non-relativistic quantum mechanics. *Rev. Mod. Phys.* **1948**, *20*, 367-387.
- 38. Feynman, R. P.; Hibbs, A. R., *Quantum Mechanics and Path Integrals*. McGraw-Hill: New York, 1965.
- 39. Feynman, R. P.; Vernon, F. L., The theory of a general quantum system interacting with a linear dissipative system. *Ann. Phys.* **1963**, *24*, 118-173.
- 40. Makri, N., Modular path integral: Quantum dynamics via sequential necklace linking. *J. Chem. Phys.* **2018**, *148*, 101101.
- 41. Makri, N., Modular path integral methodology for real-time quantum dynamics. *J. Chem. Phys.* **2018,** *149*, 214108.
- 42. Kundu, S.; Makri, N., Modular path integral for finite-temperature dynamics of extended systems with intramolecular vibrations. *J. Chem. Phys.* **2020**, *153*, 044124.

- 43. Makri, N., Small matrix disentanglement of the path integral: overcoming the exponential tensor scaling with memory length. *J. Chem. Phys.* **2020,** *152*, 041104.
- 44. Makri, N., Small matrix path integral for system-bath dynamics. *Journal of Chemical Theory and Computation* **2020**, *16*, 4038–4049.
- 45. Makri, N., Small matrix path integral with extended memory. *J. Chem. Theory and Comput.* **2021,** *17*, 1-6.
- 46. Bose, A.; Makri, N., All-mode quantum-classical path integral simulation of bacteriochlorophyll dimer exciton-vibration dynamics *J. Phys. Chem.* **2020**, *124*, 5028-5038.
- 47. Kundu, S.; Makri, N., Real-time path integral simulation of exciton-vibration dynamics in light-harvesting bacteriochlorophyll aggregates. *J. Phys. Chem. Lett.* **2020**, *11*, 8783-8789.
- 48. Kundu, S.; Makri, N., Exciton-vibration dynamics in J-aggregates of a perylene bisimide from real-time path integral calculations. *J. Phys. Chem. C* **2021**, *125*, 201-210.
- 49. Kundu, S.; Makri, N., Origin of vibrational features in the excitation energy transfer dynamics of perylene bisimide J-aggregates. *J. Chem. Phys.* **2021**, (154), 114301.
- 50. Kundu, S.; Makri, N., Electronic-vibrational density evolution in a perylene bisimide dimer: mechanistic insights into excitation energy transfer. *Phys. Chem. Chem. Phys.* **2021**, *23*, 15503-15514.
- 51. Roy, P. P.; Kundu, S.; Valdiviezo, J.; Bullard, G.; Fletcher, J. T.; Liu, R.; Yang, S., Jr.; Zhang, P.; Beratan, D. N.; Therien, et. al., Synthetic Control of Exciton Dynamics in Bioinspired Cofacial Porphyrin Dimers. *Journal of the American Chemical Society* **2022**, *144*, 6298–6310.
- 52. Dani, R.; Makri, N., Quantum quench and coherent-incoherent dynamics of Ising chains interacting with dissipative baths. *J. Chem. Phys.* **2021**, *155*, 234705.
- 53. May, V.; Kühn, O., *Charge and energy transfer dynamics in molecular systems*. 3rd ed.; Wiley: 2011.
- 54. Kundu, S.; Makri, N., Time evolution of bath properties in spin-boson dynamics. *J. Phys. Chem. B* **2021**, *125*, 8137–8151
- 55. Caldeira, A. O.; Leggett, A. J., Path integral approach to quantum Brownian motion. *Physica A* **1983**, *121*, 587-616.
- 56. Leggett, A. J.; Chakravarty, S.; Dorsey, A. T.; Fisher, M. P. A.; Garg, A.; Zwerger, M., Dynamics of the dissipative two-state system. *Rev. Mod. Phys.* **1987**, *59*, 1-85.
- 57. Frenkel, J., On the transformation of light into heat in solids. *Phys. Rev.* **1931,** *37*, 17.
- 58. May, V.; Kuhn, O., Theory of charge and energy transfer in molecular systems. Wiley: 1999.
- 59. Makri, N., Improved Feynman propagators on a grid and non-adiabatic corrections within the path integral framework. *Chem. Phys. Lett.* **1992**, *193*, 435-444.
- 60. Makri, N., Numerical path integral techniques for long-time quantum dynamics of dissipative systems. *J. Math. Phys.* **1995,** *36*, 2430-2456.
- 61. Kundu, S.; Dani, R.; Makri, N., B800-to-B850 relaxation of excitation energy in bacterial light harvesting: All-state, all-mode path integral simulations. *J. Chem. Phys.* **2022**, in press.